Proceedings
Of
The

8th International Conference
on Appropriate Technology
Songhaï Center,
Porto-Novo, Benin

November 22-25, 2018

Endogenous Knowledge, Appropriate Technology and Innovation:
Linking the Past and the Future

Gibela-TUT Partnership
Rail Manufacturing and Skills Development

International Network on Appropriate Technology (INAT)
www.appropriatetech.net

SECTION : ENERGY AND CONSTRUCTION

Edited by

J.Trimble, J. Gwamuri, B. Stephenson

International Planning Committee

A. Bakhiet, Sudan
J. Bemley, USA
H.Carwell,USA
M. Castro, Puerto Rico
T. Dalgety, Guyana
C. M. Fadel, Senegal
J. Fortunak, USA
J. Gwamuri, Zimbabwe
G. Kadoda, Sudan
J. Kiplagat, Kenya
M. K-Schutz, Namibia
K. Madzima, RSA
E. Marks, Guyana
C. Mubaiwa, Botswana
M. Muchie, RSA
A. B. Nyoni, Zimbabwe
K. Ngige, Kenya
M. Poe, USA
D. Soumonni, RSA
B. Stephenson, USA
V. Sivasubramanian, India
A. Tejansie, Liberia
J. Tharakan, USA
J. Thomas, India
J. Trimble, USA
C. Verharen, USA
M. Zami, KSA

Local Organizing Committee

A. Segla
M. Adjeran
V. Agon

TABLE OF CONTENTS

Energy and Construction Oral Presentation Papers

Utilization of Wastewater Sludge for Lightweight Concrete

Mojapelo, K. S.[1], Kupolati, W. K.[1*], Ndambuki, J. M.[1], Ibrahim, I. D.[2], Adeboje, A. O.[1], Kambole, C.[1]

[1]*Department of Civil Engineering, Tshwane University of Technology, Pretoria 0001, South Africa.*
[2]*Department of Mechanical Engineering, Mechatronics and Industrial design, Tshwane University of Technology, Pretoria 0001, South Africa.*
*Corresponding author: kupolatiwk@tut.ac.za

Abstract:
The increasing population has resulted in higher generation of domestic and industrial wastewater sludge. The sludge ends up as landfill in designated areas, which makes the land unusable. The search for lightweight materials for construction has led to the use of sludge as a viable replacement for the basic composition of concrete, due its low density. The dry sludge collected from Polokwane Waste Water Treatment Works in Limpopo Province was used as partial replacement of sand in concrete. The sludge content in sand was varied from 2.5, 5, 7.5, 10, to 12.5%. The outcomes of the analysis indicate that the addition of dry sludge in concrete mix is viable and effective. The result showed that up to 7.5% of sand can be replaced with dry sludge in concrete for structural applications. In addition, the use of dry sludge as partial replacement of fine aggregate in concrete has little or no effect on the environment.

Keywords: Wastewater, dry sludge, heavy metals, concrete composites
Paper category: Knowledge and technology transfer

INTRODUCTION

Concrete is a basic engineering material used in most civil engineering structures. Its popularity as a basic building material in construction is linked to its strength, cost effectiveness, good durability and ability to be manufactured on site. The ability to mould concrete into any shape and size, because of its plasticity in its fresh stage and its subsequent hardening to achieve strength, makes it particularly useful; therefore, there is a high dependence on concrete for construction of various infrastructures all over the world. However, the cost of concrete in developing countries has increased drastically in the past two decades due to high demand and production cost in the construction industry and this has necessitated finding alternative materials for concrete composite production. These materials could be used to partially replace cement, sand and/or stone. One of the materials used as partial replacement in concrete is sewage sludge. Tantawy et al. (2012) defined sewage as the collection of wastewater effluents from domestic, hospital, commercial and industrial establishment, and rain water. The objective of sewage treatment is to produce treated sewage water and sewage sludge suitable for safe discharge into the environment, or for reuse. The most common treatment options for sewage sludge include anaerobic digestion, aerobic digestion and composting.

Snyman et al. (2004) reported that most wastewater treatment plants in South Africa dispose of their sewage sludge on dedicated land disposal (DLD) sites (also known as sacrificial lands), since this is the quickest and cheapest way to dispose of it. Tantawy et al. (2012) stated that in the past decades, sewage sludge was primarily disposed on the land (landfill) and in sea waters. Space limitations for existing landfills and increasing environmental concerns such as groundwater pollution from land leachate, odor emission and soil contamination have prompted investigation of alternative disposal route. In trying to make good and practical use of this material, and to reduce the hazardous effect on the environment and reduce landfill, sewage sludge was introduced into concrete as part of the

basic components. Yagüe et al. (2005) reported that the performance of concrete containing dry sludge depends on sludge composition, organic material content and volume of incorporation. Sludge has been reported to be a viable composition in concrete (Sogancioglu et al. 2013; Lynn et al. 2015; Asadollahfardi et al. 2016); thus, there is the need to further research the optimal design method for the incorporation of sludge in concrete and the areas of suitable application.

MATERIALS AND METHOD

Materials

The water used for this research is potable tap water, free of substance such as chlorides, alkalis, salt, acids, sugar and other organic or chemical contents that may adversely affect the properties (durability and strength) of the concrete. The water quality was in accordance with South African National Standards (SANS) 1215:2008. The cement used was PPC SUREBUILD CEM II 42,5N. The cement was supplied by Dada's World of Hardware, Polokwane, South Africa. The coarse aggregate (quartzite) of 19 mm and fine aggregate used were supplied by Alpha sand, Polokwane, South Africa. The dry sludge used for this research was collected from the Polokwane Wastewater Treatment Plant, South Africa. The sludge was air dried and crushed until it could pass through a 4.75 mm sieve.

Safety on Wastewater Sludge Handling

Wastewater sludge is very hazardous, hence proper handling procedures need to be put in place. Direct or physical contact should be avoided and inhaling of the material must be prevented. In order to maintain proper handling of the material, some basic precautions must be followed throughout the experiment, including but not limited to the use of gloves, glasses, dust mask, safety shoes and protective clothing.

Aggregates and Dry Sludge

Aggregates

Aggregates in this case, refer to coarse aggregate and fine aggregate (natural sand and sludge). For the sake of this research, characterization of the aggregates was done to determine the physical properties. The sieve analysis was conducted to determine the dust content in the fine and coarse aggregates and the fineness modulus (FM) of the sand, in accordance with SANS 3001-AG1:2014. The geometry of the coarse aggregate such as roughness, flatness, roundness, size and shape were determined by visual assessment. Relative density was determined according to SANS 5844:2006 and these properties were used in determining the mix design for the concrete. Compacted Bulk Density (CBD) of fine and coarse aggregates was conducted in accordance with SANS 5845:2006.

Dry sludge

The dry sludge was characterized using two different methods -- the Scanning Electron Microscope (SEM) and Energy Dispersive X-ray (EDX) method and the X-ray Diffraction (XRD) analysis method. These methods helped to get a better morphology of the toxic and non-toxic elements contained in the sludge.

Scanning Electron Microscope (SEM) and Energy Dispersive X-ray (EDX)

The dry sludge was pulverized into fine particles and placed under a focused beam of high energy electron to produce stimulations that revealed information about the sample material. The morphology of the dry sludge and the concrete samples was revealed by this method. The chemical elements present were also confirmed by the EDX analysis, using a SEM (JEOL JSM-7500F, Germany) with an accelerating voltage of 15 kV. The hardened samples of the concrete, with and without sludge, were also examined using SEM. A small

piece of the sample was cut and polished for better surface finish before it was mounted on the machine for analysis.

X-ray Diffraction (XRD) analysis

The structure of the pulverized dry sludge was studied with a wide-angle X-ray diffraction (WAXD, Pan Analytical Xpert Pro diffractometer, The Netherlands), using a CuKα radiation with a wavelength of 0.154 nm at a voltage of 45 kV and a current of 40 mA.

Design strength of concrete

When developing a mix design for concrete, there is always a Target Design Strength (TDS) in mind. This TDS help to categorise which range the concrete falls into, which could be low strength (≤20 MPa), medium strength (20 – 25 MPa) or high strength (>25 MPa). This strength will inform the ratio of the cement, sand, stone and water level. Concrete containing other components other than the general natural aggregates tend to show low strength. Concrete with compressive strength greater than 25 MPa after 28 days is applicable for structural applications according to Mbadie et al. (2013). Due to the lower density of the sludge, a lightweight concrete will be used. For this research work, the design strength was 25 MPa, making it applicable for lightweight, high-strength structural application. The TDS was determined using a standard deviation of 3 MPa.

$$TDS = CS + 1.64(SD) \quad (1)$$

Where *TDS* is the target design strength, *CS* is the characteristic strength and *SD* is the standard deviation.

Methods

The water cement ratio (w/c) of 0.65 was adopted, based on the trial mix. The concrete was hand mixed in line with SANS 5861-1:2006. Based on the mix design in Table 1, a trial mix was carried out and the optimal mix was adopted. The sand partial replacement with dry sludge ranging between 2.5, 5, 7.5, 10 and 12.5%, represented by C1, C2, C3, C4 and C5 respectively, was done. Concrete cube compacting was done using the vibrating table method. The cast cubes were allowed to set on a non-vibrating floor and covered with polyethylene bags to prevent rapid evaporation. The cubes were cured in wastewater and potable water and were crushed after 7, 14, 28 and 90 days. The temperature of the water bath where the concrete cubes were cured was maintained between 23 and 25 ^{o}C.

Table 1: Sample composition for one cubic of concrete

Sample	**Stone (kg/m^3)**	**Cement (kg/m^3)**	**Sand (kg/m^3)**	**Dry sludge (kg/m^3)**	**Water (l/m^3)**
Control	1080	357	662	0	231
C1	1080	357	646	16.55	231
C2	1080	357	629	33.1	231
C3	1080	403	501	40.58	262
C4	1080	403	487	54.1	262
C5	1080	403	451	64.37	262

Mixing, casting and curing of cubes

The fine (sludge and sand) was first mixed thoroughly with the cement until a uniform homogeneous colour was attained; the coarse aggregate was then added and was thoroughly mixed until the coarse aggregate was homogeneously dispersed in the mixture. Finally, potable water was added and was thoroughly mixed until a homogeneous colour was observed.

RESULTS AND DISCUSSION

The basic components of concrete include coarse aggregate, fine aggregate, cement and water. In the study, wastewater sludge was added as part of the concrete component. The various components such as coarse and fine aggregates were characterized to verify their properties. These characterizations include physical properties and sieve analysis. Figures 1 and 2 give the sieve analysis for fine and coarse aggregates, respectively. From the analysis the materials are within allowable limit for such application.

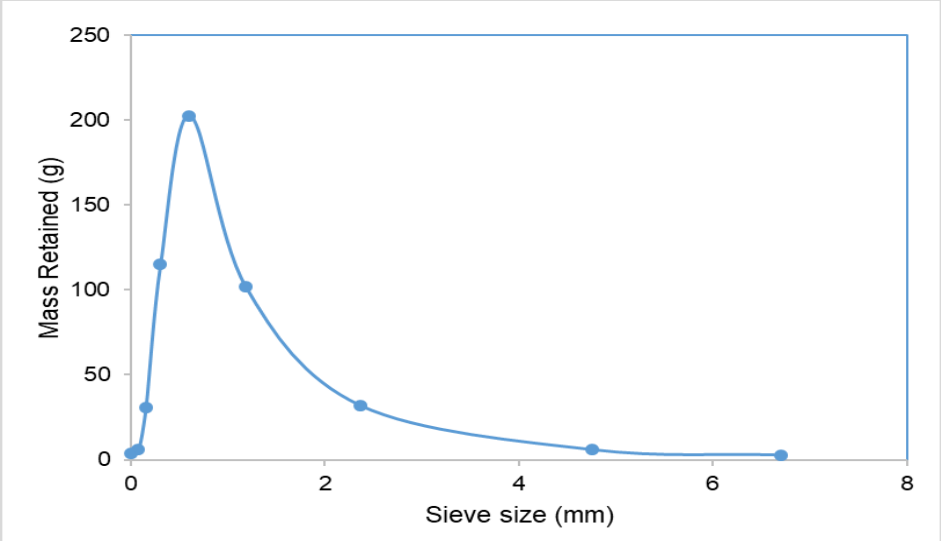

Figure 1: Sieve analysis of fine aggregate

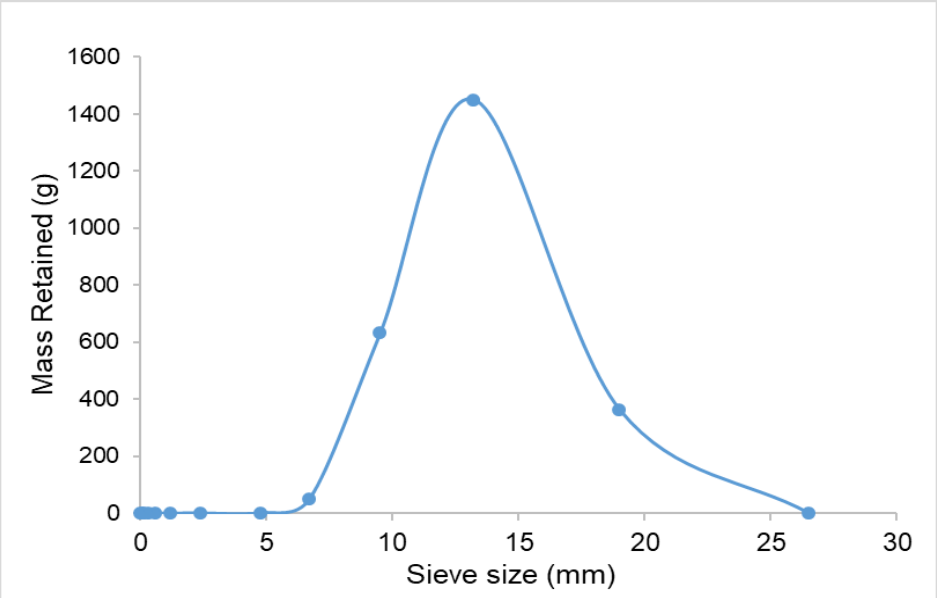

Figure 2: Sieve analysis of coarse aggregate

Physical properties

The physical properties of both the coarse aggregate and fine aggregate are shown in Table 2. The properties were determined according to the respective SANS standards. The properties that were determined include relative density, compacted bulk density, surface texture and particle shape.

Table 2: Physical properties of fine and coarse aggregate

Test	Sample	Results	Standard methods
Relative density	Stone	2.700	SANS 3001-AG23:2012
	Sand	2.629	
Compacted bulk density	Stone	1545 kg/m^3	
	Sand	1439 kg/m^3	
Surface texture	Stone	Rough	Visual analysis
	Sand	Rough, fine	
Particle shape	Stone	Irregular, angular	Visual analysis
	Sand	Irregular	

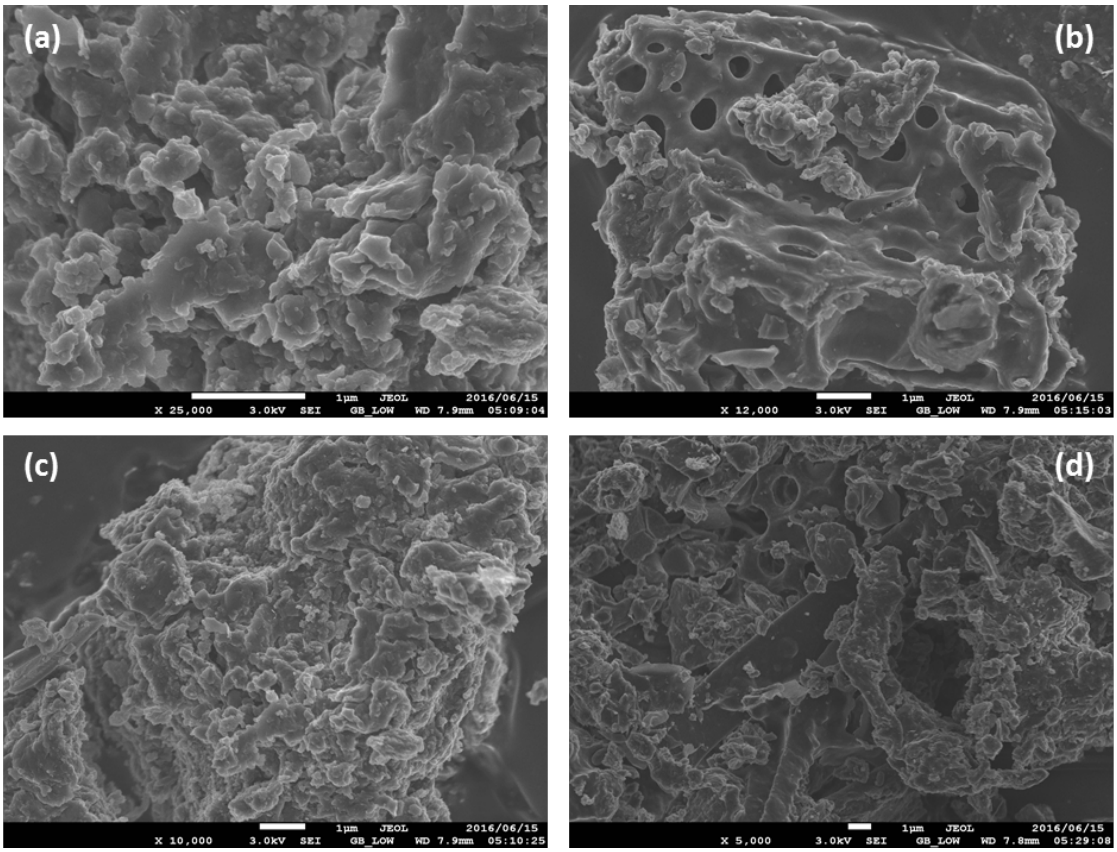

Figure 3: SEM of dry sludge at (a) x25000, (b) x12000, (c) x10000 and (d) x5000

Characterization of Dry Sludge

The microstructure of dry sludge is shown in Figures 3 and 4. The study was done at three different magnifications of 1µm, 10µm and 100nm. Figure 3 reveals the spongy nature and irregular shape of the dry sludge; these characteristics have been reported to contribute to the high-water requirement for concrete composite with partial replacement of the basic ingredient or component with wastewater sludge (Naamane et al. 2016). At a higher magnification of 100nm, Figure 4b further reveals the surface morphology of the dry sludge shape irregularity and particle distribution. A similar result on the shape irregularity was reported by Tempest and Pando (2013). They also reported that the sludge has angular particles with deep porous and rough surface, which was also observed in Figure 4.

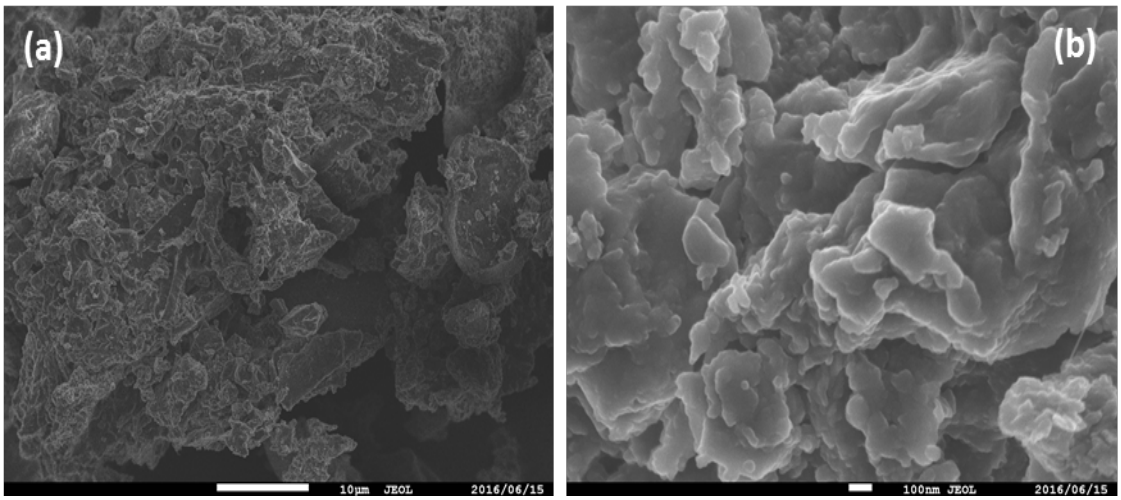

Figure 4: Morphology of dry sludge at (a) 10µm and (b) 100nm

Characterization of Concrete Sample, with and Without Sludge

Microstructure of sludge-based concrete composites

The SEM was done for better interpretation of the trends in the morphological characteristic of the concrete composites, as it relates to the compressive strength of the concrete composites. The SEM micrographs were recorded at various magnifications for an in-depth understanding. Figures 5 and 6 show the SEM images for samples of 0, 2.5, 5, 7.5 and 12.5% sand replacement with dry sludge.

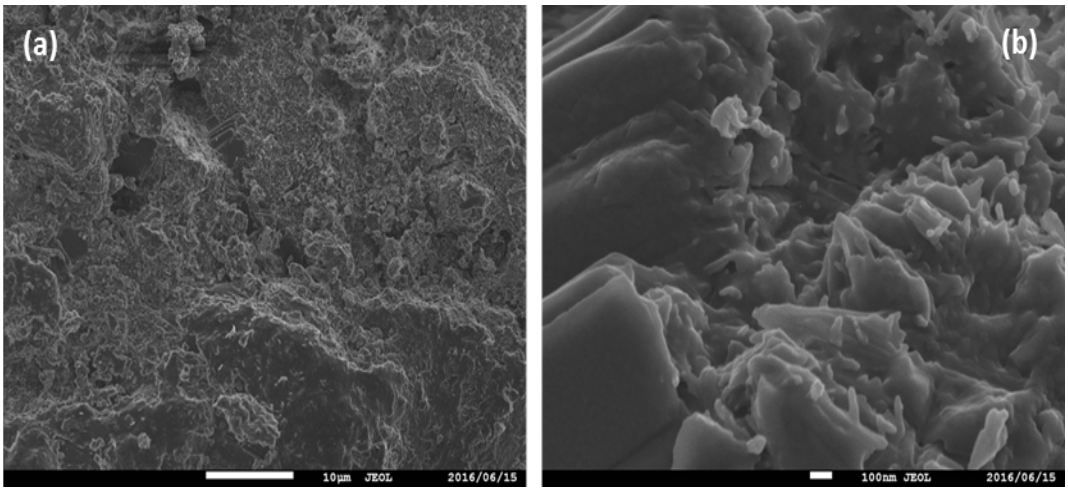

Figure 5: Morphology of concrete composite without sludge at (a) 10µm and (b) 100nm

The morphology of the control sample of concrete composite without any addition of sludge is shown in Figure 5. The sample is observed to be well compacted due to the cementitious material and the quality of the sand. In Figure 6a, the surface microstructure of the 2.5% sand replacement is almost like that of the control sample. This is as a result of the small content of sludge in the mix; hence, close compressive strength was observed for both mixes (Sogancioglu et al. 2013; Lynn et al. 2015). Concrete composites containing more sludge content (Figure 6) shows more void between crystals when compared to the control sample; this may have resulted in the reduction in compressive strength of the concrete. Similar observation was reported by Asadollahfardi et al. (2016), where concrete was produced and cured with domestic wastewater. The micrographs show the presence of organic matter, which appears spongy in nature. This morphology will have a convincing impact on the water demand, the porosity and the compressive strength of the concrete produced. Similar effect of sludge on water demand was reported by Monzo et al. (2003) and Naamane et al. (2016).

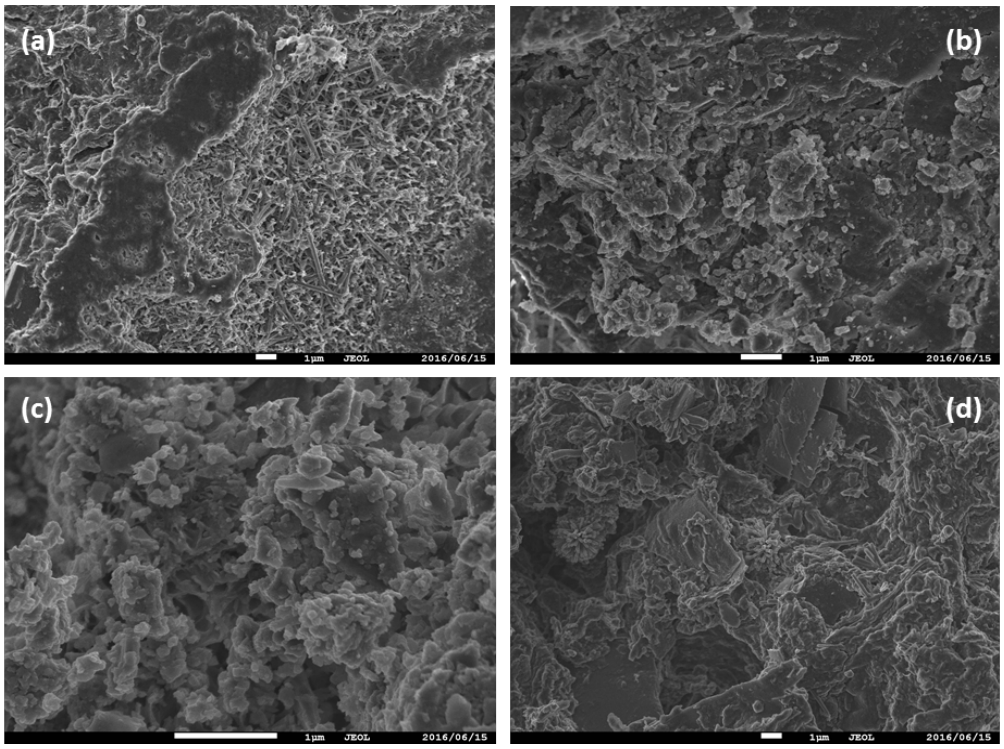

Figure 6: SEM images of concrete composites of: (a) 2.5%, (b) 5%, (c) 7.5% and (d) 12.5% sand replacement with dry sludge

Energy dispersive X-ray (EDX) of sludge-based concrete composites

The elemental contents of the concrete samples are presented in Tables 3 and 4. Based on the EDX results, the amount of oxygen and calcium were observed to have increased, which could be as a result of the introduction of sludge. It has been reported that incorporation of wastewater tends to increase the percentage of certain elements in the concrete. Asadollahfardi et al. (2016) reported that the sulfur, chlorine and sodium contents increased slightly with the addition of treated wastewater before chlorination.

Table 3: EDX quantitative percentages of elements in concrete without sludge

Element name	Formula	Weight (%)	Atom (%)	Compound (%)
Carbon	C	8.73	15.77	8.73
Oxygen	O	39.72	53.84	39.72
Magnesium	Mg	0.82	0.73	0.82
Alluminium	Al	1.74	1.40	1.74
Silicon	Si	8.97	6.92	8.97
Sulfur	S	0.71	0.48	0.71
Calcium	Ca	36.59	19.80	36.59
Iron	Fe	2.71	1.05	2.71
Total		100.00	100.00	100.00

Table 4: EDX quantitative percentages of elements in concrete with sludge

Element name	Formula	Weight (%)	Atom (%)	Compound (%)
2.5% Sand Replacement				
Carbon	C	7.74	14.04	7.74
Oxygen	O	41.31	56.24	41.31
Magnesium	Mg	0.81	0.73	0.81
Aluminium	Al	1.84	1.49	1.84
Silicon	Si	6.47	5.02	6.47
Sulfur	S	0.58	0.40	0.58
Potassium	K	0.43	0.24	0.43
Calcium	Ca	38.64	21.00	38.64
Iron	Fe	2.17	0.85	2.17
Total		100.00	100.00	100.00

5% Sand Replacement				
Carbon	C	11.03	18.25	11.03
Oxygen	O	47.12	58.55	47.12
Sodium	Na	0.63	0.54	0.63
Magnesium	Mg	0.71	0.58	0.71
Aluminium	Al	2.17	1.60	2.17
Silicon	Si	7.87	5.57	7.87
Sulfur	S	0.47	0.29	0.47
Potassium	K	0.42	0.21	0.42
Calcium	Ca	27.66	13.72	27.66
Iron	Fe	1.93	0.69	1.93
Total		100.00	100.00	100.00
12.5% Sand Replacement				
Carbon	C	15.37	24.06	15.37
Oxygen	O	48.65	57.17	48.65
Magnesium	Mg	1.02	0.79	1.02
Aluminium	Al	1.91	1.33	1.91
Silicon	Si	6.18	4.14	6.18
Phosphorus	P	0.15	0.09	0.15
Sulfur	S	0.75	0.44	0.75
Potassium	K	0.18	0.09	0.18
Calcium	Ca	24.25	11.38	24.25
Iron	Fe	1.53	0.52	1.53
Total		100.00	100.00	100.00

Compressive strength of concrete cured in potable water

The concrete samples were compacted using vibrating table method to remove air bubbles, eliminating any potential voids that could lead to a reduction in compressive strength. The cubes were cured in potable water. The results are shown in Figure 7. The results show that the vibrating method was effective. In a reported by Alqedra et al. (2011), similar patterns were observed.

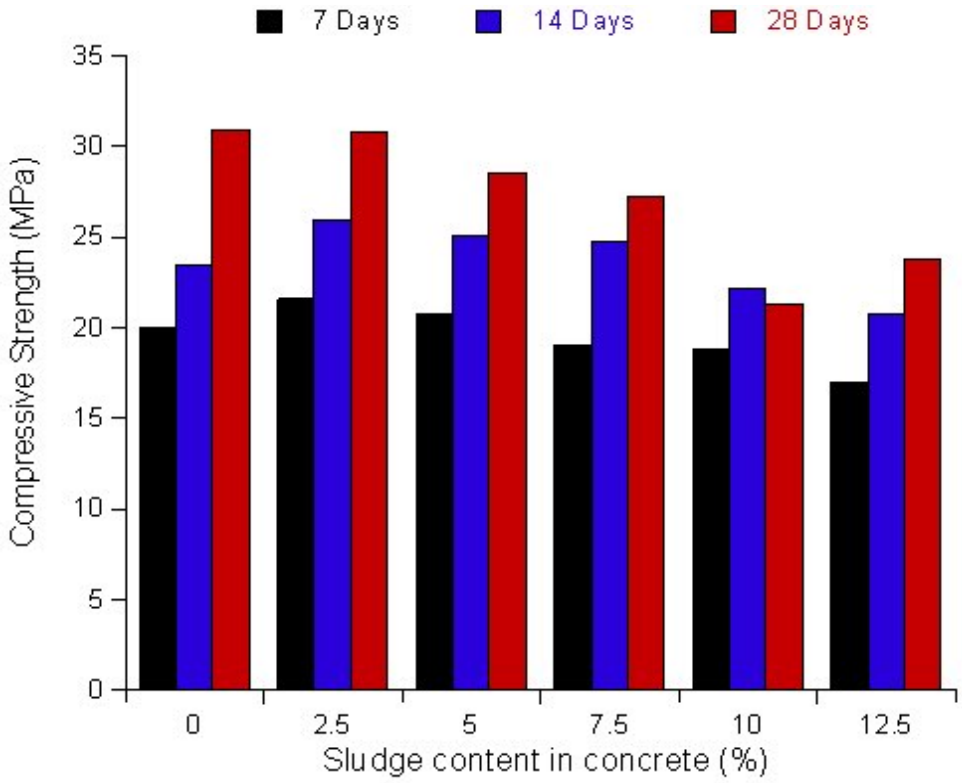

Figure 7: Compressive strength of concrete samples cured in potable water

Effect of wastewater sludge-based concrete on the environment

From Table 5, some heavy metals such as Chromium (Cr), Cupper (Cu), Cadmium (Cd), Lead (Pb) and Zinc (Zn) were observed to be seeping out of the concrete. Hence, the amount of seepage was compared with standards to ensure it was not above the allowable quantity. Based on South Africa guidelines for the utilization and disposal of wastewater sludge prepared for Department of Water Affairs and Forestry, the heavy metal seepage was within the allowable limit (see Table 5). In a report by Tchounwou et al. (2014), it was reported that metals such as magnesium (Mg), copper (Cu), nickel (Ni), iron (Fe), chromium (Cr) and zinc (Zn) are required essential nutrients for various physiological and biochemical functions. Varieties of deficiency syndromes or diseases are as a result of inadequate supplies of these basic micro-nutrients (WHO/FAO/IAEA, 1996); hence, the metal seepage can be considered as non-hazardous to plant and animal and in general, the environment. The concentration of metals in sludge is usually reduced significantly in concrete composite; this confirms the possible decrease in environmental impact of sludge as basic component in concrete composite (Sales et al. 2010; Sales et al. 2011).

Table 5: Allowable metal limits for South African wastewater sludge (Snyman and Herselman, 2006)

Heavy metal	**Allowable limit (mg/kg)**	**Current research (mg/l)**
Arsenic (As)	< 40	-
Cadmium (Cd)	< 40	< 0.92
Chromium (Cr)	< 1200	< 0.02
Copper (Cu)	< 1500	< 0.07
Lead (Pb)	< 300	< 0.09
Mercury (Hg)	< 15	-
Nickel (Ni)	< 420	< 0.02
Zinc (Zn)	< 2800	< 0.01

CONCLUSIONS

In this study, the effect of sludge in concrete as partial replacement for sand was tested. Air-dried sludge was used to replicate a typical site condition and then crushed until it passes through 4.74 mm sieve. The effect of curing medium on the compressive strength of concrete after 7, 14 and 28 day was investigated. Based on the result, the following conclusions are drawn:

i) The addition of dry sludge influenced the properties of the concrete in the fresh and curing stage.

ii) Sand content in concrete can be replaced up to 7.5% with dry wastewater sludge for structural applications.

iii) The water analysis shows that sludge seepage from the concrete composites is within the allowable limit.

Acknowledgment

I would like to thank TUT for providing platform to carry out this research. I also wish to acknowledge the financial support received from SML projects, Polokwane, South Africa.

References

Alqedra M., Arafa M. and Mattar M. (2011). Influence of low and high organic waste water Sludge on physical and mechanical properties of concrete mix. Journal of Environmental Science and Technology 4(4):354–365.

Asadollahfardi G., Delnavaz M., Rashnoiee V. and N. Ghonabadi. (2016). Use of treated domestic wastewater before chlorination to produce and cure concrete. Construction and Building Materials 105:253–261.

Jamshidi M., Jamshidi A. and Mehrdadi N. (2012). Application of Sewage Dry Sludge in Concrete Mixtures. Asian Journal of Civil engineering (Building and housing) 13(3):365–375.

Lynn C.J., Dhir R.K., Ghataora G.S. and R.P. West. (2015). Sewage sludge ash characteristics and potential for use in concrete. Construction and Building Materials 98:767–779

Mbadie W.T., Kupolati W.K., Ndambuki J.M. and E.R. Sadiku. 2013. Beneficial use of waste glass as partial substitute for cement and aggregates in concrete. MTech Thesis. Tshwane University of Technology Pretoria, South Africa.

Monzo J., Paya J., Borrachero M.V. and I. Girbes. (2003). Reuse of sewage sludge ashes (SSA) in cement mixtures: the effect of SSA on the workability of cement mortars. Waste Management 23:373–381.

Naamane S., Rais Z. and M. Taleb. (2016). The effectiveness of the incineration of sewage sludge on the evolution of physicochemical and mechanical properties of Portland cement. Construction and Building Materials 112:783–789.

Sales A., de Souza F.R., dos Santos W.N. and Almeida F.D.R. (2011). Mechanical properties of concrete produced with a composite of water treatment sludge and sawdust. Construction and Building Materials 25:2793–2798.

Sales A., de Souza F.R., dos Santos W.N., Zimer A.M. and Almeida F.D.R. (2010). Lightweight composite concrete produced with water treatment sludge and sawdust: Thermal properties and potential application. Construction and Building Materials 24:2446–2453.

Snyman H.G. and J.E. Herselman. (2006). Guidelines for the utilization and disposal of wastewater sludge. Water Research Commission (WRC). WRC Report No. 261/06.

Snyman, H.G., Herselman, J.E. & Kasselman. G. (2004). WRC Report on the Project "A metal content survey of South African sewage sludge and an evaluation of analytical methods for their determination in sludge. Report No. 1283/1//04 ISBN No. 1-77005-225-9

Sogancioglu M., Yel E. and U.S. Yilmaz-Keskin. (2013). Utilization of andesite processing wastewater treatment sludge as admixture in concrete mix. Construction and Building Materials 46:150–155.

Tantawy M.A., EI-Roudi A.M., Elham M.abdalla and Abdelzaher M.A., (2012) Evaluation of pozzolanic activity of sewage sludge ash

Tchounwou P.B., Yedjou C.G., Patlolla A.K. and D.J. Sutton. (2014). Heavy Metals Toxicity and the Environment. NIH Public Access. DOI:10.1007/978-3-7643-8340-4_6

Tempest B.Q. and M.A. Pando. (2013). Characterization and Demonstration of Reuse Applications of Sewage Sludge Ash. International Journal of Geomate 4(2):552–559.

WHO/FAO/IAEA. World Health Organization. Switzerland: Geneva. (1996). Trace elements in Human Nutrition and Health.

Yague A., Valls S., Vazquez E. and Albarea F. (2005). Durability of concrete with addition of dry sludge from waste water treatment plants Cement and Concrete Research 35:1064–1073.

DESIGN OF A PV (PHOTOVOLTAIC) MICRO-GRID /TEST-BED SYSTEM FOR NUST

Emmanuel Manikwa, Mufaro Tapera, Nothando Ndlovu

and Jephias Gwamuri*

Department of Applied Physics, National University of Science & Technology, Bulawayo, Zimbabwe

***Jephias.gwamuri@nust.ac.zw**

ABSTRACT

Failure to invest in newer means of generating power has resulted in decreased power generation in the backdrop of a subsequent increase in demand for power in Zimbabwe. To mitigate problems associated with energy shortages in the country which is affecting the proper running of institutions of higher learning including NUST, a PV micro-grid system was designed to that effect. An energy audit was carried out to assess the institution's energy consumption and a site assessment was conducted to help assess the feasibility of the system. System design was then carried out. HOMER Pro, an industry standard tool for simulating and optimizing hybrid microgrid systems was used to size the stand-alone and grid-tied systems. Sensitivity analysis was performed to predict the influence of scaled output, depth of discharge and slope of PV modules on the output and cost of the system. It was observed from the results that a grid-tied, micro-grid system rated at 500 kW would be the most cost-effective option (compared to the stand-alone) with a net present value (NPV) which is 73% less. The grid-tied system was evaluated to have a payback period of approximately 7 years.

Key Words: Grid-tied, Stand-alone, HOMER Pro, Micro-grid.

Paper Category: Energy

1. INTRODUCTION

The availability of an accessible, clean, reliable and environmentally friendly supply of energy that meets the demand of the population of any one country is necessary not only for its economic growth but for the general improved standard of living for its citizens (Jager et al. 2014). Most countries in the world are facing energy problems and Zimbabwe is no exception. Zimbabwe's recorded peak demand stands at 2200 MW (RECP, 2016) while its current demand is a 1600 MW against a production of 1250 MW. This has resulted in a national shortfall of 670 MW as presented by table 1.

Table 1 Power generation statistics for Zimbabwe (*Source*: ZETDC website).

Power Station	Installed capacity (MW)	Actual Generation (MW)	Percentage Generation (%)
Kariba South	750	716	96
Hwange	920	506	55
Harare	80	0	0
Munyati	80	10	12.5
Bulawayo	90	12	13
Total	1920	1250	65

The perennial power deficit has been caused by obsolete machinery which have outlived their life spans. These result in frequent power cuts which negatively affects the running of the university and damages equipment. Increasing investments on the currently available power generating technologies will solve the power deficit problem for a short while. Conventional sources of energy such as coal have a disadvantage of producing carbon dioxide which negatively impacts the environment (Jager et al, 2014). A more sensible and long-lasting solution would be to invest heavily in a green energy supply which would help create a future not only for the people of Zimbabwe but for the whole Southern African region. PV systems on the other hand play the greatest role in alleviating energy crisis and reducing pollution to the environment systems (Nandar et al, 2016). This project was carried out as an initiative to increase energy security through the use of a clean, accessible, reliable, environmentally friendly and sustainable energy supply (Gwamuri and Mhlanga, 2010).

2. SYSTEM DESCRIPTION

A micro-grid system is a local energy grid which has the ability to disconnect from the traditional grid and operate autonomously. It enables power to be generated locally for local load and can comprise of various power generating sources which are mostly renewable energy generators such as solar modules and wind turbines and are usually accompanied by some form of energy storage which makes it highly flexible and efficient. Extra system components besides PV modules which are necessary for a PV system are termed balance of system components (BOS). System components needed for any one system are dependent on whether the system is grid-tied or stand-alone. BOS components include mounting structure, energy storage, DC-DC converters/ inverters or DC-AC converters, cables etc.

2.1 PV Modules

Photovoltaics is the field of technology and research based on the photovoltaic effect. Devices based on the photovoltaic (PV) effect generate a potential in response to incident electromagnetic radiation (Jager et al, 2014). The solar cell is the basic building block of PV devices. A number of cells are electrically connected to each other to make up a photovoltaic module which is usually mounted in a single support structure. These can be wired together to form an array which is a source of DC electricity. PV systems can either be stand-alone or grid-tied. Stand-alone PV systems are autonomous systems that are operated without the grid and thus rely on solar power only. Grid-tied systems on the other hand are connected to the grid via an inverter which converts DC power to AC electricity. PV systems tilt angle with the horizontal has an impact on the amount of radiation received by the system and hence affects the output of the system (Khoo et al, 2014). Taking the site latitude as tilt angle for solar modules produces optimum results (Guo et al, 2016).

2.3 Inverters

An inverter's circuit design has an effect on the output wave which can be square wave, modified sine wave, pulsed sine wave, or sine wave. The two dominant commercialized waveform types of inverters as of 2007 are modified sine wave and sine wave (Gohil et al, 2017)). An inverter converts DC power from the PV modules to AC power which can be used by electrical appliances. The inverter is a major component of any PV system (grid-tied or stand-alone) and so has an impact on the overall performance of the PV system (Vignola, 2007).

2.4 Batteries

The battery bank is considered the weakest link of any PV system that includes batteries as they need maintenance, replacement every five (5) years which significantly affects the overall efficiency and cost of the system (Osaretin and Edeko 2015). The energy stored in the batteries is used when there is little or no sunlight usually at night but sometimes during the day, during discharge the stored chemical energy is converted to electrical energy which powers up electrical loads. For PV applications, deep cycle batteries are used which discharge small amounts of current for a long period of time e.g. at night or during a black out (Gohil, 2017).

2.5 Charge Controller

It is a switching device that goes between the solar modules and the batteries whose function is to connect (and disconnect) the charger to the battery bank (Gohil et al, 2017). As the name suggest, a charge controller regulates charge going in and out of batteries. It operates the battery within its operation limits hence protects the battery bank from overcharging and over discharging (Tarang, 2016; Nandar, 2016). Regularly equalizing charge and informing the user on the status of the system are some of the functions of the charge controller (Islam, 2015). Pulse width modulation (PWM) and maximum power point tracking (MPPT) are the most commonly used charging strategies and are advantageous in that they adjust rates of charging depending on the bank's maximum capacity and also monitor the battery temperature to prevent overheating (Osaretin and Edeko, 2015).

2.6 Sizing/Modelling tools

The HOMER Pro Micro-power Optimization Model is a computer model developed by the U.S. National Renewable Energy Laboratory (NREL) to assist in the design of hybrid micro-power systems and to facilitate the comparison of power generation technologies across a wide range of applications. HOMER simplifies the task of designing grid-tied and stand-alone power systems for many applications. Total costs of installing and operating a system over its life time are modelled using the tool. HOMER allows comparison of many different design options based on their technical and economic merits. It also assists in understanding and quantifying the effects of uncertainty or changes in the inputs. HOMER performs three principal tasks: simulation, optimization, and sensitivity analysis and so working effectively with HOMER requires understanding of its three core capabilities simulation, optimization, and sensitivity analysis and how they interact (Gurupira and Rix, 2017).

3. METHODOLOGY

To achieve the designing of the different micro-grid systems the project was divided into three phases feasibility study, system modelling and system optimization. Feasibility study involved site assessment to estimate the quantity of sun resources and area available for the solar system. This step allowed the determination of whether the system would be able to supply the institution (NUST) with adequate power at the selected site. Shading from trees and buildings near the site were also assessed. The following equations were used to predict the solar potential for the area available for system installation:

$$Number\ of\ solar\ modules = \frac{Area\ available\ for\ Solar\ Plant}{Area\ of\ one\ solar\ module} \quad (1)$$

$$\text{Total power output} = Total\ area \times solar\ irradiance \times Conversion\ eff \quad (2)$$

Equation 1 was used to calculate the number of solar modules the area could carry.
An energy audit was then carried out which provided information on how much power the institution was consuming. System design was based on the daily consumption which was obtained from the energy audit. A simple method of conducting an energy audit for a tertiary institution such as NUST is to analyze monthly electricity bills. The following equations were used to calculate the yearly and daily consumption.

$$\text{Yearly consumption (kWh)} = \sum Monthly\ consumptions(KWh) \quad (3)$$

$$Daily\ consumption\ (kWh) = \frac{Yearly\ Consumption(KWh)}{12 \times months \times 30\ days} \quad (4)$$

3.1 System sizing

System sizing involved hand sizing and system modelling. Hand sizing provided a general idea of the system size and then system modelling using HOMER Pro applied the practical system parameters found at the site to get a system that will provide for the NUST load.

3.1.1 Hand Sizing

The first part of system sizing was carried out to give a general idea of the system size as mentioned above. Different means of determining the size of each system component were used.

3.1.1.1 PV Module sizing

The institution's monthly electricity bills were used to calculate an estimate of the system size using the steps given below;

i. Separated the monthly consumption according to seasons i.e. (summer and winter).
ii. Calculated the daily average (KWh) from the monthly electrical bills.
iii. Divided by the solar insolation of the area to get the system size in KW.
iv. Divided by the derating factor (0.80) which takes into account the system's overall efficiency such as soiling and imperfect electrical connections.

Electricity consumption varies based on the season hence it was necessary to size systems based on the seasons so that the season with the highest consumption is put into consideration.

3.1.1.2 Inverter Sizing

The right size of the inverter is necessary for any one system to make sure that adequate power reaches all the appliances being run at the same time. To determine the size of the inverter to be used for this system the following equation was used;

$$\text{Inverter size} = Load + 30\%(Load) \quad (5)$$

3.1.1.3 Battery Bank Sizing

Batteries are very important when it comes to solar systems as they ensure that in times when the sun is down and in weather conditions that do not favour solar energy the load will always be supplied by adequate power. Batteries should never be consistently undercharged and should never be completely drained. It is best to size the battery bank so that it gets regularly charged to capacity. To calculate the size of the battery bank, the following steps were used;

a. Voltage Selection e.g. 12V, 24V, 48V.
b. Calculate the number of daily watt-hours and use the value to calculate the Average Daily Amp hrs.

$$Average\ daily\ Amp\ hrs = \frac{AC\ Average\ Load \times Temperature\ Compensation}{Inverter\ Efficiency} \quad (6)$$

c. Average Daily Amp hrs multiplied by Days of autonomy to get Amp hours.

$$Total\ Amp\ hrs = \frac{Amp\ hours}{0.5 \times (Depth\ of\ Discharge)} \quad (7)$$

e. Divide the total Amp hrs by selected battery capacity to get the number of batteries in parallel.

3.1.1.4 Charge Controller

A charge controller, limits the rate at which electric current is added to or drawn from electric batteries. It prevents overcharging and protects against overvoltage, which can reduce battery performance or lifespan, and may pose a safety risk. To calculate the size of a charge controller the following equation was used,

$$\textit{Size of charge controller} = Output\ of\ Solar\ system + 25\%(Output\ of\ solar\ system) \quad (8)$$

3.1.2 System Modelling

HOMER (Hybrid Optimization of Multiple Electric Renewables), was designed to simplify the assessment of both stand-alone and grid-tied power systems for a variety of applications. HOMER Pro models the total cost of installing and operating a power system (the Net Payment Cost) over its life span also allowing the modeler to compare many different design options based on their technical and economic merits. HOMER Pro also assists in understanding and quantifying the effects of uncertainty or changes in the inputs hence helping overcome challenges encountered in the design of micro-grid systems due to a large number of design options and the uncertainty in key parameters e.g. load size.

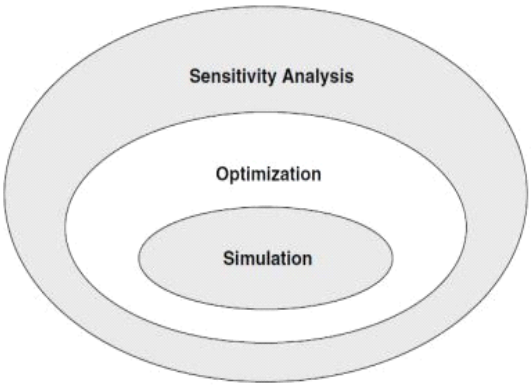

Figure 1: Conceptual relationship between simulation, optimization, and sensitivity analysis (Lambert, 2006).

The simulation oval shown in figure 1 is contained or enclosed in the optimization oval and similarly the optimization oval is contained or enclosed in the sensitivity analysis oval this means that a single optimization consists of multiple simulations and the same applies to a single sensitivity analysis which is made up of multiple optimizations (Lambert, 2006).

4. RESULTS AND ANALYSIS

This section gives the results of both the hand sized and simulated systems. Firstly, results of the site assessment are presented and there after results of the hand sized systems are presented to guide the researcher on the approximate system size. Simulation results from HOMER Pro are given at the end of this section.

4.1 Feasibility study

NUST is located at latitude 20.2 degrees and longitude 28.6 degrees. The location has an average insolation of 6.28 kWh/m^2/day according to NASA. Insolation has an impact on system size as it gives the amount of electromagnetic radiation or solar energy received at the location specified by the longitude and latitude values of the area. More sunlight means more current is produced by the solar cells but in the event of excessive insolation, the cells begin to experience high temperatures which generally reduces the power output of the solar cell.

Approximately seven (7) hectares/ 70,000 m^2 is available for installation of a solar system at the site. Using a standard 300 W solar module with the following specifications: length = 1,675 mm, width = 1,001 mm, peak conversion efficiency = 17.89% and solar irradiance (for a surface perpendicular to the sun's rays at sea level on a clear day) = 1,000 W/m^2. From the given land area, the number of solar modules that could be installed at the site were estimated to be 41,750 using equation (1) and the total solar output was evaluated to be 12.5 MW using equation (2).

4.2 Energy Audit

Monthly electricity consumption kWh values were obtained and are given in Table 2. The data shows that the month with maximum consumption was May and one with the least was January.

Table 2: Monthly energy consumption from October 2016 to September 2017

Month	Consumption kWh
October	61690
November	56689
December	47570
January	43260
February	55840
March	57150
April	54150
May	64080
June	60190
July	59410
August	57040
September	63200

The data given in the table was used in the sizing of the different micro-grid system. Using equation (3), yearly consumption was evaluated at 680,269 kWh, whilst daily consumption was calculated to be 1889.6 kWh using equation (4).

4.3 System sizing

4.3.1 Hand sizing

The daily energy consumption for winter (May to August) was calculated to be 1,957.1 kWh and that for summer (September -April) was calculated to be 1808.8 kWh. The values given above show that winter has the highest daily consumption. Insolation data of 5

kWh/m^2/day and 6.2 kWh/ m^2/day were used to evaluate the winter and summer peak consumptions respectively. The peak power consumption for winter was evaluated to be 490 kW and the peak consumption for summer was 365 kW. The peak consumption for winter was then selected to be the overall system size with ~490 kW.

The different components were sized using 81.5 kW as the daily load and 1,957.1 kWh as the daily consumption. Grid- tied system do not have batteries and charge controllers as they use the grid as their back up. The steps and equations found in section 3.1.1 were used to hand size the different grid-tied and stand-alone systems. The different system components are given in table 3.

Table 3: Summary of different components of stand-alone and grid-tied systems

Component	Stand-alone	Grid-tied
PV Modules size(kW)	430	430
Inverter size (kW)	103	103
Battery Bank(kA-h)	245	--
Charge Controller (kW)	600	--

4.3.2 System Modelling

Using the load data obtained from the energy audit, the monthly consumption values were averaged to get hourly load values these were used as input into HOMER Pro and simulations were done based on what was the current energy consumption of the institution. Figure 2a and 2b shows how the different system components for both the stand-alone and the grid-tied systems were interconnected.

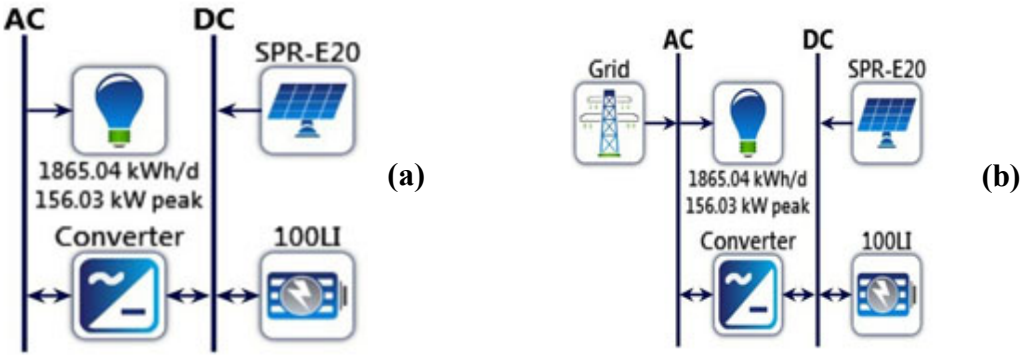

Figure 2: Showing **(a)** layout of a stand-alone system, and (**b)** a layout of a grid-tied system

Table 4 gives a summary of the system components that make up the stand-alone and grid-tied systems.

Table 4: Summary of the different specifications for both the stand-alone and the grid-tied systems.

	Stand-alone	**Grid-tied**
PV (kW)	500	500
Storage (Generic 100KWh Li-Ion) (Strings)	76	1
System converter (kW)	368	165
Grid (kW)	---	400
Excess electricity (%)	13%	0.470
Capital ($M)	5.82	0.7

For the stand-alone system, the PV system was designed to produce a maximum of 872,469 kWh/year which makes up 100% of the system's electrical supply. As shown on Table 4 the standalone system has large battery bank which is used to store extra power generated by the system for use at night when the PV modules cannot produce power. Simulations done on HOMER reveal that an increase in the PV system to 1200 kW reduces the number of batteries that are needed for this application by 26 also reducing the cost of the system by almost 2.5M. This increase is accompanied by an increase in excess electricity of up to 65% the value produced in a year. Thus, the system will have been over sized and excess energy will not be used since this is a standalone system. Increasing the number of batteries reduces the excess electricity to 13% which is still a large value.

A grid- tied system on the other hand with the same size of PV as the standalone but with an option of selling to and buying from the grid produced a maximum of 872,469 kWh/year and had very little excess electricity and unmet load. Thus, for the grid-tied system when modules produce more than enough power the excess is sold back to the grid and when the modules produce less than what the system needs additional power will be bought from the grid.

Figure 3 reveals how electricity production is distributed for the stand-alone and grid-tied systems. Since a stand-alone system has no grid purchases, 100% of its energy needs are from the solar modules. A grid-tied system on the other hand has PV which makes up 69.5% of the energy production and the grid makes up 30.5% of the power (grid purchases (381,992 kWh/year)). For both systems i.e. grid-tied and stand-alone, the size of the photovoltaic system employed were the same. With a maximum output of 451kW for a rated capacity of 500kW. PV/renewable penetration of 128%. Period of operation of the solar modules for a year were given as 4,413 hrs.

(a)

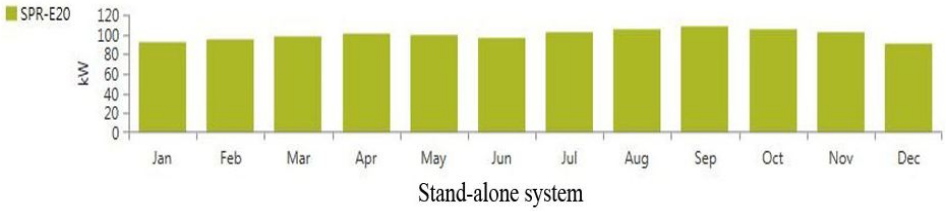

Stand-alone system

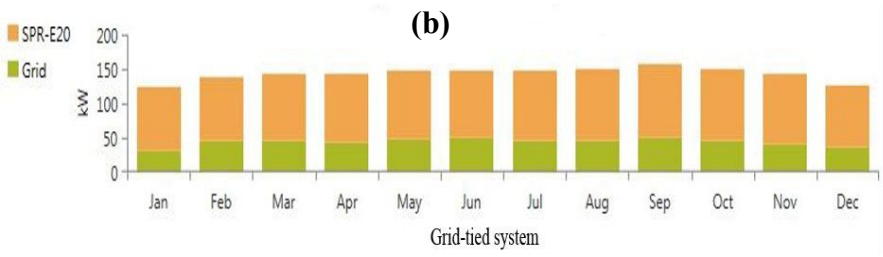

Figure 3: Summary of the monthly electrical production; **(a)** Stand-alone system and, **(b)** Grid-tied system

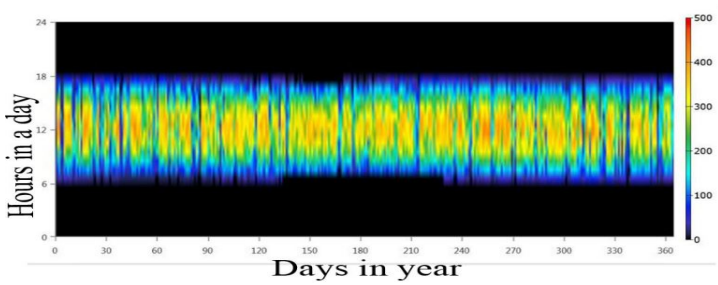

Figure 4: Daily PV outputs for both the Grid-tied and the Stand-alone systems (24 hrs/day for 1 year).

The graph in figure 4 shows the output of the PV modules for a 24 hours per day. The graph also shows how the output of the PV varies throughout the year for the 365 days of the year. The graph shows that between 6pm and slightly above the sixth hour of the morning there is no output from the solar modules since there wouldn't be any sunlight available during that time of the day. Power is only realised between 6am and 6pm. Figure 5, shows that grid purchases for a grid tied system were done at night and on some rare occasions during the day this could have been due to weather.

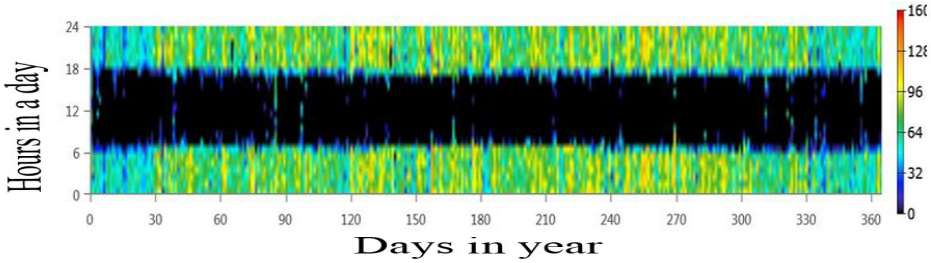

Figure 5: Grid purchases during night: – System not running.

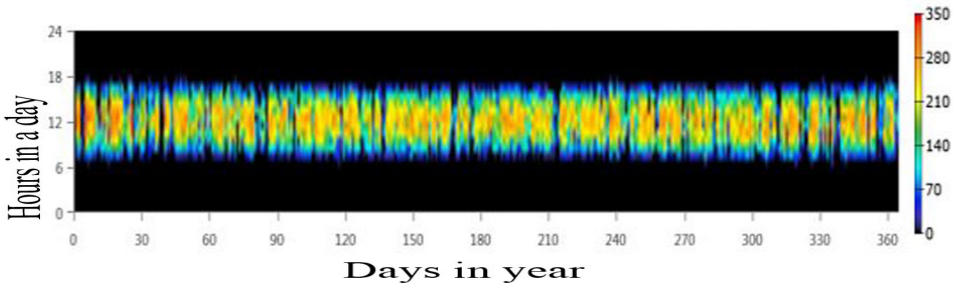

Figure 6: Grid sales: - System producing excess electricity.

Figure 6 shows energy that was sold to the grid. Excess energy made during the day is sold back to the grid in a grid-tied system. This allows for a great deal of saving. Table 4 shows that the stand-alone system was designed to have 76 Generic 100 kWh Li-Ion batteries which were to be used when the PV modules were not producing anything i.e. at night and during days of little or no sunlight. Minimum state of charge was set at 30% of maximum capacity of the battery bank and set point of batteries during charging was set at 100%. The standalone system had Batteries were sized to produce 65.5 hrs of autonomy with an expected life of 15years. Energy into the batteries per year was valued at 444,555 kWh and energy out per year 401,944 kWh. Thus, batteries experience losses due to system inefficiencies and internal resistances of the batteries.

The standalone system also comprised of an inverter with a capacity of 165 kW. The inverter operates 8758 hrs per year hence will need periodic checking (O&M). Energy output of the inverter was sized at 680,410 kW. Energy input for the inverter 716,221 kWh/year and experiences losses of 35,811 kWh/year. System also has a MPPT (Maximum Power Point Tracker) which converts DC power from the PV modules to a constant DC which can be sent to batteries for charging and also to the inverter for conversion to AC to provide power to the Load. System has no DC load and hence has no need for a rectifier.

The grid tied system on the hand just had one 100 kWh Li-Ion. With an expected life of 15 years. With an inverter of maximum output of 368 kW. The inverter in the grid-tied system works for 4,417 hrs/year which is almost half of the hours worked by the inverter used in the standalone system this is because the inverter in the stand-alone system converts power from the PV modules and power from the batteries at night whilst one used in the grid-tied system only converts during the day.

5. CONCLUSSIONS AND RECOMMENDATIONS

Net Present Cost (of a component) gives the present value of all the costs of installing and operating the component over the project lifetime, minus the present value of all the revenues that it earns over the project lifetime. HOMER calculates the net present cost of each component in the system, and of the system as a whole. Costs include capital costs, replacement costs, O&M costs, fuel costs, emissions penalties, and the costs of buying power from the grid. Revenues include salvage value and grid sales revenue. The NPC of installing the designed stand-alone system was calculated to be $8.39M more than the designed grid-tied system.

Though the designed systems had the same PV capacity and maximum output the stand-alone system needed a battery bank to store up charge for use at a later time when the PV modules were no longer producing power. The designed standalone system was limited to a capacity of only 500 kW to make sure that all the power produced by the system was used to serve the load. Scaling up the PV system produced a system with less batteries and hence less cost but this system would be having a large value of excess electricity (system over sized). To avoid over sizing the system, the PV had to be limited and battery bank scaled up as a result.

Of the sensitivity variables considered, scaling up the load by 30% had an impact on the system size and cost of the grid-tied system whereas the standalone system was affected by the scaling up and variation of minimum state of discharge of the batteries. Generally, PV systems require large capital injections and minimum maintenance and operation costs for the life time of the system. What affects the rate of returns for either grid-tied and standalone system is the size of the system and how excess electricity is dealt with.

The sized Grid-tied system was found to cost less when compared to the stand-alone system. Size and NPC of the grid tied system is exaggerated by the inclusion of the battery

and charge controller. Results reveal that the capital needed to implement the grid-tied system is 631,473 and system payback time will be 7 years. The stand-alone system requires $5 million to implement and its payback time is way above system life time hence the grid-tied is cost effective. What increases the cost of the stand-alone system is the inclusion of the battery bank. The NPC of the system of a stand-alone system is considerably higher due to the presence of a battery bank that requires to be changed at least three times during the life-time of the system. The same system can be designed using HOMER Grid for comparison as HOMER Grid has the capability to design a grid-tied system without back -up.

REFERENCES

Jäger. K, Isabella. Ol, Smets. H. M. A, van Swaaij R. A.C.M.M, Zeman, M. 2014. *Solar Energy: Fundamentals, Technology, and Systems*. Delft University of Technology, Delft, Netherlands.

Energy sector in Zimbabwe Report, 2016. Available at: https://www.business-sweden.se/globalassets/energy-sector-in-zimbabwe.pdf. Accessed: 20 Aug 2018.

ZETDC Background. Available at: http://www.zesa.co.zw/index.php/2012-12-12-10-37-20/zetdc. Accessed: 20 Aug 2018.

Nandar, O, Kyaw, S. L, Hla, M.T. 2016. *A Charge Controller Design for Solar Power System.* IJSTR, vol, 5, pp 71-75.

Gwamuri, J, Mhlanga, S. 2010. *Design of PV solar home system for use in urban Zimbabwe.* 4th International Appropriate Technology Conference, Accra, Ghana.

Khoo, Y. S, Nobre, A, Malhotra, R, Yang, D, Ruther, R, Reindl, T, Aberle, A.G, 2014. *Optimal Orientation and Tilt Angle for Maximizing in-Plane Solar Irradiation for PV Applications in Singapore*. IEEE Journal of Photovoltaics, Vol. 4, No. 2.

Guo. M, Zang, H, Gao, S, Chen, T, Xiao J, Cheng, L, Wei, Z, Sun, G. 2017. *Determination of the Optimal Tilt Angle of Solar Collectors for Different Climates of China.* Appl. Sci., 7, 1028; doi:10.3390/app7101028

Gohil, P. B, Jadav, D. P, Katakiya, C. N, Zala, J. B. 2017. *Solar Battery Charger.* IJEDR, Vol 5(2) ISSN: 2321-9939.

Vignola, F, Mavromatakis, F, Krumsick, J. 2008. *Perfomance of PV inverters* in Solar 2008, 37th American Solar Energy Society Annual Conference, Vol 1, pp 628, May 3-8, San Diego, California.

Osaretin, C. A, and Edeko, F. O. 2015. *Design and Implementation of a Solar Charge Controller with Variable Output*. Journal of Electrical and Electronic Engineering Vol 12, No 2, ISSN 1118 – 5058.

Thakur, T. 2016. *Solar Power Charge Controller*. Global Journal of Researches in Engineering: Electrical and Electronics Engineering, Vol 16(8), Online ISSN: 2249-4596 & Print ISSN: 0975-5861

Islam, M. S, 2015. *Thin Film Solar Charge Controller: A Research Paper for Commercialization of Thin Film Solar Cell.* Advances in Energy and Power Vol. 3(2) pp 29-60.

Gurupi, T and Rix, A. J. 2017. *PV Simulation software comparisons: PVSYST, NREL SAM AND PVLIB*, SAUPEC 2017 Conference.

Lambert, T, Gilman, P, Lilienthal, P. 2006. *Micropower System Modeling with HOMER* in Integration of Alternative Sources of Energy by Farret, F. A, and Simoes M. G. John Wiley & Sons, pp.379-418.

Development of a Smart Multi Feedstock Biodiesel Plant

Ilesanmi Afolabi Daniyan[1] PhD
[1]Department of Industrial Engineering, Tshwane University of Technology, Pretoria, South Africa.
afolabiilesanmi@yahoo.com
Emmanuel Bello[2] PhD
[2]Department of Mechanical Engineering, Federal University of Technology, Akure, Nigeria.
Tunde Ogedengbe[3] PhD
[3] Department of Mechanical Engineering, Federal University of Technology, Akure, Nigeria.
tioged@yahoo.com
Pius Mogaji[4] PhD
[4] Department of Mechanical Engineering Federal University of Technology, Akure, Nigeria.
pbmogaji@yahoo.com
Khumbulani Mpofu[1] PhD
[1]Department of Industrial Engineering, Tshwane University of Technology, Pretoria, South Africa.
mpofuk@tutu.ac.za

Abstract
The quest for increased energy security and the need to develop renewable alternatives to fossil fuel has brought about the development of renewable sources of energy. In this study, a biodiesel processing plant was designed and fabricated for producing biodiesel from used and unused oils. The developed plant consists of nine sections namely; oil storage, methanol storage, water tank, mixing tank, reactor, wash tank, separating section, glycerol storage and biodiesel storage. The plant majorly consists of three 3 kW variable speed sparkless electric motor, three 2.5 kW pumps, 220 V AC alarm, four flow switches, 220 V timer relay, 60 A contactor, 3 thermostatically controlled 300 kW electric heater, sawdust insulation, 12 ball valves, 3 thermostats, a separating funnel, shaft and a stirrer of diameter 25 mm with seven blades that rotate in the reactor. The stirrer is driven by the 3 kW electric motor. The plant was designed to have an output capacity of 200 litres per day. A stainless steel of 2.5 mm thickness was used in the fabrication of the tanks for each of the nine sections of the plant because of its excellent combination of high strength, formability and corrosion resistance. Performance evaluation of the plant was carried out using used frying oil and palm olein oil. The biodiesels produced were characterized and its properties compared in respect of the American Society for Testing and Materials (ASTM D6751) and EN 14214 limits for biodiesel. This study provides a smart and cost-effective plant for processing biodiesel from different feedstock as well as the plants' associated design data which could serve as a template for scaling its development.

Keywords: biodiesel, energy, feedstock, fossil fuel, reactor
Paper category: Energy

1. INTRODUCTION

Fossil oils are fuels which come from ancient animals and microorganisms. Fossil fuel formation requires millions of years, thus, belong to non-renewable energy sources. The growth of the population is not covered by domestic crude oil production (Demirbas, 2009; Bull, 1996). An increase in the oil price often leads to economic recessions, as well as global and international conflicts. Especially in some developing countries, the great development in the economy in fossil fuel resources will be consumed in only 65 more years. In addition, the

emission produced by the combustion of fossil fuels also contributes to the air pollution and global warming. (Agarwal, 2007; Prabhakar and Elder, 2009). Most countries also experience more and more international pressure on global warming issue (Vandenbroucke, 1985). Renewable and clean alternative fuels have received increasing attention for current and future utilization. Biodiesel as one promising alternative to fossil fuel for diesel engines has become increasingly important due to environmental consequences of petroleum-fueled diesel engines and the decreasing petroleum resources. Biodiesel can be produced by chemically combining any natural oil and fat with an alcohol such as methanol or ethanol (Udeh, 2017; Tuly *et al.,* 2017). Methanol has been the most commonly used alcohol in the commercial production of biodiesel. Lots of researches on biodiesel have shown that the fuel made by vegetable oil can be used properly on diesel engines (Apostolakou *et al.,* 2009; Pedrojevic, 2008). In fact, the energy density of biodiesel is quite close to regular diesel. Biodiesel can be produced from soybean, need seed oil or waste cooking oil with methanol via transesterification in the presence of acid or base catalysts (Hamze *et al.,* 2015; Abbah *et al.,* 2016). Similarities between the combustion properties of biodiesel and petroleum-derived diesel have made the former one of the most promising renewable and sustainable fuels for the automobile (Benjumea *et al.,* 2008). Used oil is a prospective alternative for biodiesel production as it helps solve disposal problems and a substantial amount of biodiesel can be produced from it, representing one of the better alternatives to reuse and dispose cooking oil efficiently and economically (Felizardo *et al.,* 2006). According to Bello (2008), biodiesel can be produced from coconut oil, palm oil etc. However, high demand of diesel fuel and the availability of waste cooking oil indicate that biodiesel from used oil cannot completely replace fossil diesel fuel but can contribute to reduce the dependency on petrol based diesel (Martin and Grossman, 2011). Marjanovic *et al.* (2010) also developed a batch reactor for the production of biodiesel from divers feedstock but the analysis of integration features of the overall process for biodiesel production was a missing link. Bello *et al.* (2013) developed a batch biodiesel processor that can transesterify used and unused oil to biodiesel. The batch processor cannot be used in the production of large volume of biodiesel since its capacity is limited to 20 litres per day, therefore it is not efficient to operate large production in a continuous mode. Also, Highina *et al.* (2012) reported on biodiesel production using J*atropha curcas* oil in a batch reactor in the presence of zinc oxide as catalyst. The reactor is limited to single feed and use of heterogeneous catalyst only.

2. MATERIALS AND METHOD

The components of each section and their functions are given in the Table 1.

Table 1: Plant units, function and components

S/N	Unit	Function	Components
1.	Oil Tank	Storage of used oil	Cylindrical tank, inlet valve and outlet valve, electric heater, filter, flow meter, temperature sensor and regulator.
2.	Methanol tank	Storage of methanol	Cylindrical tank, inlet valve and outlet valve
3.	Water tank	Storage of distilled water	Cylindrical tank, inlet valve and outlet valve
4.	Mixing tank	Mixing methanol and catalyst	Cylindrical tank, electric motor, stirrer, diameter shaft, inlet valve and outlet valve, flow meter, temperature sensor and regulator.
5.	Reactor	Transesterifying used oil to biodiesel	Cylindrical tank, electric motor, heater, stirrer, diameter shaft, temperature sensor and

			regulator, flow meter, filter, inlet valve and outlet valve and pump
6.	Wash tank	Washing biodiesel in purification process	Cylindrical tank, inlet valve and outlet valve, flow meter and pump
7.	Separating column	Separating glycerol from biodiesel	Separating funnel, inlet valve and outlet valve, pump
8.	Glycerol tank	Storage of by product: Glycerol	Cylindrical tank, inlet valve and outlet valve
9.	Biodiesel tank	Storage the main product: biodiesel	Cylindrical tank, inlet valve and outlet valve

2.1 Design for tank orientation

The daily production is calculated as 200 litres and the targeted design output of the reaction tank is 6.7m^3, hence, the volume of the mixing tank is designed to 7.0 m^3 capacity for chances of overflow.

The volume of the reaction tank (cylinder) is given as Equation 1.

$$V = \pi r^2 h \qquad (1)$$

where:

Volume V= 7.0 m^3 (Targeted output)

For buoyancy and balance, tank height is assumed to be twice its diameter ($h = 2D$), Equation 1 becomes

$$V = \pi \times 0.5D^2 \times 2D$$
$$D^3 = \frac{4V}{2\pi}$$
$$D^3 = \frac{4 \times 7}{2 \times 3.142}$$
$$D = 1.65\ m$$
$$Since\ h = 2D$$
$$h = 3.3\ m$$

The tank diameter D and height h is calculated as 1.65 m and 3.3 m respectively. According to Khurmi (2010), the maximum tensile strength of steel plate (AISI 1020) is given as 215 N/mm^2. Using a safety factor of 1.5, the circumferential stress is calculated as 143.33 N/mm^2. The thickness t of the cylindrical tank is given by Equation 2.

$$t = \frac{pd}{2\sigma_c \eta} \qquad (2)$$

where:

p is the internal pressure, (N/mm^2), d is the diameter of the tank, (mm), σ_c is the circumferential stress, (N/mm^2) and η is the efficiency of joint. Using a tank diameter of 1650 mm, circumferential stress of 143.33 N/mm^2, joint efficiency of 0.9 and internal pressure of 0.4 N/mm^2 (Collusi *et al.,* 2005).

$$t = \frac{0.4 \times 1650}{2 \times 143.33 \times 0.9}$$

The thickness of the cylindrical tank from equation 6 is calculated as 2.5 mm. The plant comprises of nine cylindrical tanks. Stainless steel was selected for the fabrication of the nine cylindrical tanks because of its excellent combination of high strength, good formability and corrosion resistance.

2.2 Mixing unit

The major components of the mixing unit shown is the electric motors and the mixing tank which envelops the stirrer (i.e. shaft and blade assembly). Also included are the inlet valve, the outlet valve as well as temperature sensor and regulator. The shaft is subjected to both twisting and bending moment with negligible axial loading.

The mass of fluid was calculated as 5800 kg, therefore, the weight of the fluid is given by Equation 3.

$$W = mg \qquad (3)$$

where:

m is the mass of fluid, (kg) and g is the acceleration due to gravity (m/s^2).

The mass of fluid is calculated as 5800 kg, therefore from equation 11, the weight of fluid is 60 kN

The torsional moment acting on the shaft as given by Hall *et al.* (1980) is expressed in Equation 4.

$$M_t = \frac{kW \times 1000 \times 60}{2\pi\, rev/min} \qquad (4)$$

Using a 3 kW electric motor as reported earlier which is adequate to stir fluid of such density 800-900 kg/m^3 at a speed of 200-300 rpm. An optimum average speed of 250 rpm is adequate for this operation (Bello *et al.,* 2013).

$$P = 3\ kW, N = 250\ rpm.$$

$$M_t = \frac{3 \times 1000 \times 60}{2 \times 3.142 \times 250}$$

$$M_t = 114.6\ Nm$$

Shaft design consists of the determination of the correct shaft diameter that will ensure satisfactory rigidity and strength when the shaft transmits power under different operating and loading conditions (Hall *et al.,* 1980). For shaft with keyway (stainless steel), the allowable shear stress is given as 55 MN/m^2 (Hall *et al.,* 1980; Ashby *et al.,* 2007).

The total torque required to overcome the viscosity and shear through the mixture is given by Equation 5.

$$T = \frac{P}{2\pi N} \qquad (5)$$

where:

P is the power of the electric motor, (watts); and N is the number of revolution per sec

Using an electric motor of 3 kW at an average revolution of 250 rpm,

$$T = \frac{3 \times 10^3}{2 \times 2.143 \times 250}$$

The total resisting torque is calculated as 0.12 kN.

The shaft is solid and the formula for determining the diameter of a shaft having little or no axial loading according to Hall *et al.* (1980) is expressed as Equation 6.

$$d^3 = \frac{16}{\pi S_s}\sqrt{(K_b M_b)^2 + (K_t M_t)^2} \qquad (6)$$

where:
M_t is the torsional moment, (Nm), M_b is the bending moment, (Nm), K_b is the combined shock and fatigue factor applied to bending moment, K_t is the combined shock and fatigue factor applied to torsional moment, S_S is the allowable shear stress, (N/m^2) and d is the shaft diameter, (m).
Given the fact that the shaft of the mixing unit is to stir fluid whose maximum weight was determined to be 60 kN, using a 3 kW, 250 rpm electric motor, the torsional moment M_t on the shaft was calculated as 114.6 Nm. The shaft is subjected to twisting moment only, the bending moment M_b is zero since the shaft is vertical. The shear stress Ss for stainless steel material used for the shaft is given as 55 MN/m^2 and for rotating shaft with minor shock K_b=1.0 and $K_t = 1.0$. When these values were introduced into Equation 6 as follows;

$$d^3 = \frac{16}{3.142\times55\times10^6}\sqrt{(1.0\times114.6)^2}$$

$$d = 25\ mm.$$

The shaft diameter, d for the mixing tank is calculated as 22 mm, 25 mm to the nearest standard size. Stainless steel is preferred for the fabrication of the mixing tank and reactor because of its excellent combination of high strength, formability and corrosion resistance. The schematic of the cross section of the mixing tank a well as the baffle design for the reaction tank is shown in Figures 1.

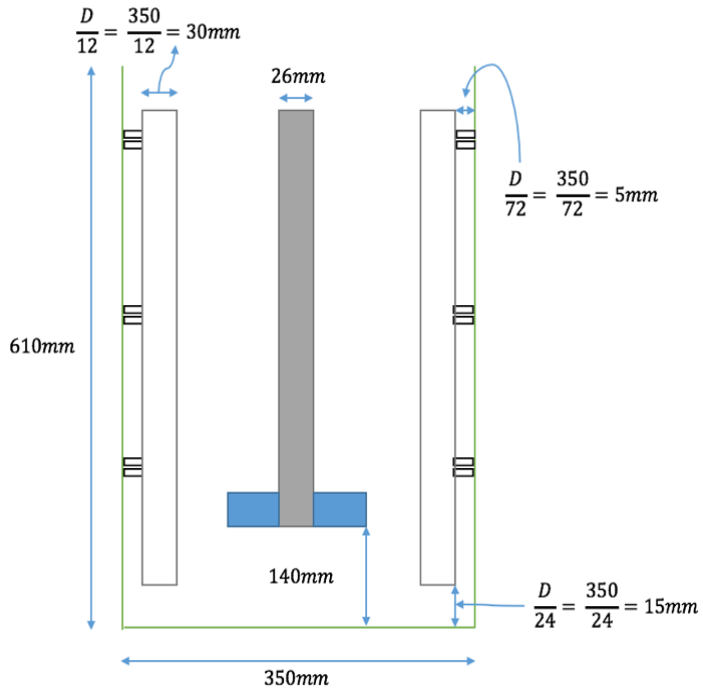

Figure 1: Cross section of the mixing tank

2.3 Description of the Developed Plant

The developed plant consists of nine sections namely: oil storage, chemical tank, mixing tank, reactor, wash tank, separating section, glycerol storage and biodiesel storage (Figure 2). There are three 3 kW variable speed sparkless electric motor, three 2.5 kW pumps, 220 V AC alarm, 4 flow switches, 220 V timer relay, 220 V, 60 A contactor, 3 thermostatically controlled 300 kW electric heater, saw dust insulation, ball valve, 3 thermostats, separating funnel, a shaft of diameter 25 mm which serves as stirrer having seven blades that rotate in the reaction chamber and mixing tank baffles to control the splashing. The stirrer is driven by the electric motor. A 2.5 mm thick stainless steel was used in the fabrication of the plant sections because of its high resistance to corrosion. The temperature of the reactor and mixing tank is controlled by means of the thermostat. The reactor consists of an in-built heater and filter. Feedstock and sodium methoxide are fed from the oil tank and mixing tank respectively into the reactor, the ON button is switched, the reactor will transesterify the raw materials to biodiesel with minimal operator interference. A float switch is located into the filtered drum to send a signal to the logic controller the amount of filtered oil. Another float switch is located in the reaction tank to indicate the amount of oil loaded into the reaction tank while the third float switch is located in the methanol/catalyst mixing tank to indicate the amount of loaded methanol. A temperature probe is attached to read and keep the temperature inside the oil storage, mixing and reaction tank in a given temperature range. The temperature probe's output is used by the logic controller to indicate when the inline heater should be engaged or disengaged. The size of the heater determines the power requirements of the plant. The major variables to be sensed in the process plant are flow, temperature, pressure (as well as differential pressure) and level. The transmitter serves as the interface between the process and its control system. The transmitter is to convert the sensor signal (millivolts, mechanical movement, pressure differential etc.) into a control signal. As the process pressure in the vessel varies from 100 to 500 kPa. This is called the range of the transmitter. The dynamic response of most transmitters is usually much faster than the process and the control valve. Hence, the transmitter is just a transducer that converts process variable to an equivalent control signal. A pressure drop transmitter is employed with an orifice plate as a flow transmitter. The pressure drop over the orifice plate (the sensor) will be converted to a control signal.

Figure 2 shows the developed plant after the fabrication process.

Figure 2: The developed biodiesel plant units

The process flow diagram for the production of biodiesel which consists of the integration of the different sections is given in Figure 3.

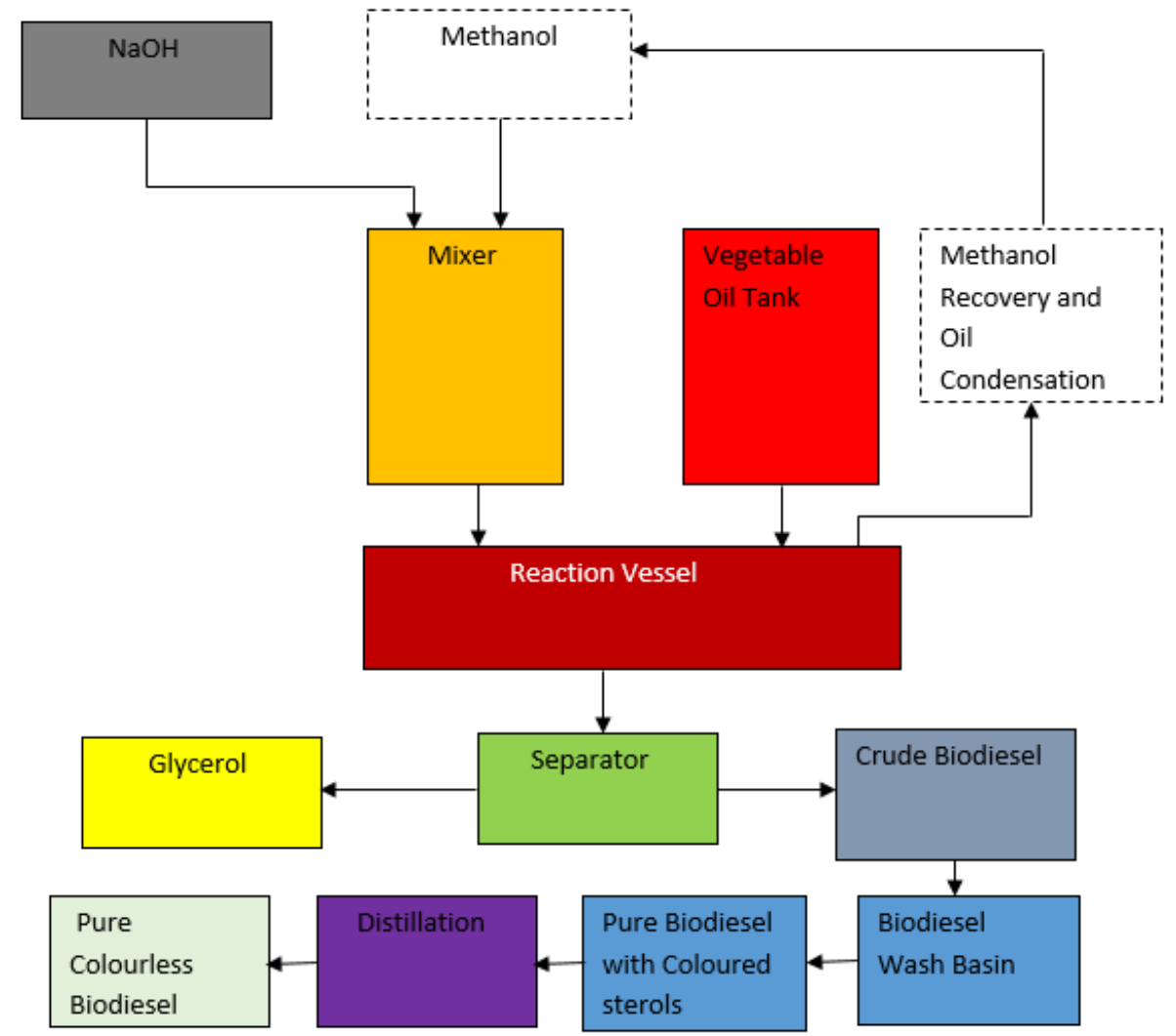

Figure 3: Process flow diagram for biodiesel production

2.4 Acid transesterification

Acid transesterification was used for converting used cooking oil to biodiesel using 99.8% pure methanol while hydrogen chloride (HCl) was used as catalyst. Waste cooking oil was filtered to remove solid particles and pre-heated at a temperature of 100℃ to remove water and other volatile impurities. Hydrogen chloride at a concentration of 1-2 wt. % was added to methanol with methanol in excess in a molar ratio ranging between 4:1 to 9:1 to oil. The mixture was gently stirred in the mixing tank for 10 minutes to form methanolic HCl. The pre-heated oil was thereafter transferred to the reactor alongside with methanolic HCl and the mixture was stirred at stirring speed ranging between 200-400 rpm and temperatures ranging between 40℃ -90℃ for 1-5 hours. The product was discharged into the separating funnel and allowed to settle for 24 hours. After the settling, the product is observed to have separated into two distinct layers; the top biodiesel and the bottom glycerol.

2.5 Alkali transesterification

Alkali transesterification was employed for the conversion of palm olein virgin oil to biodiesel with 99.8% pure methanol and sodium hydroxide (NaOH) as catalyst. Sodium hydroxide at concentrations ranging between 1-2 wt.% was first dissolved as a catalyst in methanol and mixed in the mixing tank for 30 minutes to form sodium methoxide. Pre-heated oil was transferred into the reactor where sodium methoxide from mixing tank was added to it. Continuous mixing of the mixture was done in the reactor at temperatures ranging between 40-90℃ and stir speed ranging between 200-400 rpm for 1-5 hours. This ensures the reaction is driven to completion with phase separation into two layers: the top biodiesel and the bottom glycerol. The methyl ester formed was washed with water in a volume ratio of 3:1 to remove other impurities after which it is dried by passing it through anhydrous sodium sulphate (Na_2SO_4). Both the separated biodiesel and glycerol was then transferred to the respective storage tanks for storage.

3. Results and discussion

The result obtained from the characterization of the biodiesels produced from used and unused oil is given in Table 2.

Table 2: Properties of biodiesels from used and unused oils compared to ASTM D6751 (2015) and EN 14214 standards (2015)

S/N	Property	A	B	ASTM Standard D6751	EN 14214 Standard
1.	Colour	Golden brown	Dark brown	-	-
2.	Density (kg/m^3)	909	905	800-950	860-900
3.	Specific Gravity	0.909	0.905	0.800-0.950	0.860-0.900
4.	Kinematic Viscosity (mm^2/sec)	3.80	4.30	1.9-6.0	3.5-5.0
5.	Flash Point (℃)	167	190	130 min.	101 min.
6.	Pour Point (℃)	-15	-20	-30 to -10	-
7.	Cloud Point (℃)	-5	-12	-15 to 5	
8.	Saponification value (mg NaOH/g)	107.99	122	-	-
9.	Acid value (% mass)	0.1683	0.3366	0.5 max	0.5 max
10.	Iodine value (% mass)	108	116	-	120 max
11.	Peroxide value (Meq peroxide/kg oil)	119	124	-	-

The symbol A in Table 2 represent biodiesel from Palm olein virgin oil using alkali transesterification while symbol B represent biodiesel from used oil obtained via acid transesterification.

The transparent methyl esters produced from virgin oil and used cooking and virgin oil is shown in Figures 4 and 5 respectively.

Figure 4: Biodiesel from unused oil and byproduct; glycerol.

Figure 5: Biodiesel from used oil and by product; glycerol.

4. CONCLUSIONS

A biodiesel plant with a capacity of 200 litres per hour was designed and fabricated. It can transesterify used and unused vegetable oil to biodiesel and can also undertake both alkali-catalysed and acid-catalysed transesterification. The fuel properties of biodiesels produced are within the limits of ASTM D6751 and EN 14214 standards for biodiesel and are similar to the fuel properties of fossil diesel which confirms that it can be used an alternative fuel for diesel engines without modification. This study provides a plant for processing biodiesel from different feedstock as well as the plants' associated design data which could serve as a template for scaling its development; the production of biodiesel is cost-effective and a true alternative when compared to the cost of fossil diesel.

References

Abbah, E. C., Nwandikum, G. I., Egwuonwu, C. C. and Nwakuba, N. R. (2016). Effect of Reaction Temperature on the Yield of Biodiesel from Need Seed Oil. American Journal of Energy Science 3:16-20.

Apostolaku, A. A., Kookos, I. K., Marazioti, C., and Angelopoulos, K. C. (2009). Techno-economic Analysis of a Biodiesel Production Process from Vegetable Oils. *Fuel Process. Technol.* 90:1026-1030.

Argawal, A. K. (2007). Biofuels (Alcohols and Biodiesel) Application as Fuel for Internal Combustion Engines. *Progress in Energy and Combustion Science*. 33:233-271.

American Society of Testing Materials, ASTM (2015). Standard Specification for Biodiesel Fuel Blend Stock (B100) for Middle Distillate Fuels. ASTM International West Conshohocken PA. pp. 1-10.

Ashby, M., Shercliff, H. and Cebon, D. (2007). Materials Engineering, Science, Processing and Design. Rajkamal Press, India: 21-31.

Benjumea, P.; Agudelo J. and Agudelo, A. (2008). Basic properties of palm oil biodiesel-diesel blends. *Fuel,* 87: 2069-2075.

Bello, E. I. (2008). Evaluation of Coconut Oil Methyl Esters as an Alternative Fuel for Diesel Engine. Ph.D Thesis. pp. 1-112.

Bello, E. I., Daniyan, I. A., Akinola, A. O. and Ogedengbe, T. I. (2013). Development of a Biodiesel Processor. *Research Journal in Engineering and Applied Sciences.* 2(13):182-186.

Bull, S. R. (1996). Renewable energy transportation technologies. *Renewable Energy,* 9:1019-1024.

Collusi, J. A., Borrero, E. E. and Alape, F. (2005). Biodiesel from an Alkaline Transesterification Reaction of Soybean Oil Using Ultrasonic Mixing. *JAOCS*. 82(7) 525-530.

Dube, W. O., Marc, A. A and Fred, B. (2007). Acid-Catalysed Transesterification of Canola Oil to Biodiesel under Single and Two Phase Reaction Conditions. *Energy and Fuels* 21:2450-2459.

European Norm. EN (2015). European Biodiesel Standard. pp. 1-10.

Felizardo, P., Correia, M., Raposo, I., Mendes, J., Berkemeier, R. and Bordado, J. (2006). Production of Biodiesel from Waste Frying Oil. *Waste Management*. 26: 487-494.

Hall, A. S., Holowenko, A. R. and Laughlin, H. G. (1980). Machine Design. Purdue University Press: 113-130.

Hamze, H., Akia, M. and Yazdani, F. (2015). Optimization of Biodiesel Production from Waste Cooking Oil Using Response Surface Methodology. Process Safety and Environmental Protection. 94:1-10

Highina, B. K., Bugaje, I. M. and Umar, B. (2012). Liquid Biofuel as Alternative Transport Fuel in Nigeria. *Int. Journal of Petroleum Technology Development,* 1:1-15.

Khurmi, R. S. (2010). Applied Mechanics and Strength of Materials. Chand Publishing Company, New Delhi.

Marjanovic, A. V., Stamenkovic, O. S., Todorovic, Z. B., Lazic, M. L. and Veljkovic, V. B. (2010). Kinetics of the Base-Catalysed Sunflower Oil Ethanolysis. *Fuels.* 89(3):669-671.

Martin M. and Grossman, I. E. (2011). Optimization of Heat and Water Integration for Biodiesel Production from Cooking Oil and Algae. Department of Chemical Engineering, Carnegie University, Pittsburgh. pp. 1-38.

Pedrojevic, Z. J. (2008). The Production of Biodiesel from Waste Frying Oils: A Comparison of different Purification Steps. *Fuels.* 87:3522-3528.

Prabhakar, S. V. R. K. and Elder, M. (2009). Biofuels and resource use efficiency in developing Asia: Back to basics. *Applied Energy,* 86: 30-36.

Tuly, S. S., Saha, M., Mustafi, M. M. and Sarker, M. R. I. (2017). Production and Application of Biodiesel from Waste Cooking Oil. API Conference Proceding. Vol. 1851 020030, Issue 1.

Udeh, B. A. (2017). Biodiesel Production from Waste Vegetable Oil (Sunflower) Obtained from Fried Chicken and Plantain (2017). Journal of Petroleum and Environmental Biotechnology. 7:321.